Langmuir

Article

pubs.acs.org/Langmuir

Stabilization of Thin Liquid Films by Repulsive van der Waals Force

Er Qiang Li,[†] Ivan U. Vakarelski,*[,†] Derek Y. C. Chan,[‡,§] and Sigurdur T. Thoroddsen[†]

[†]Division of Physical Sciences and Engineering & Clean Combustion Research Center, King Abdullah University of Science and Technology (KAUST), Thuwal, 23955-6900, Saudi Arabia

[‡]Department of Mathematics and Statistics, University of Melbourne, Parkville, VIC 3010, Australia

[§]Department of Chemistry and Biotechnology, Swinburne University of Technology, Hawthorn, VIC 3122, Australia

Supporting Information

ABSTRACT: Using high-speed video recording of bubble rise experiments, we study the stability of thin liquid films trapped between a rising bubble and a surfactant-free liquid−liquid meniscus interface. Using different combinations of nonpolar oils and water that are all immiscible, we investigate the extent to which film stability can be predicted by attractive and repulsive van der Waals (vdW) interactions that are indicated by the relative magnitude of the refractive indices of the liquid combinations, for example, water (refractive index, n = 1.33), perfluorohexane (n = 1.23), and tetradecane (n = 1.43). We show that, when the film-forming phase was oil (perfluorohexane or tetradecane), the stability of the film could always be predicted from the sign of the vdW interaction, with a repulsive vdW force resulting in a stable film and an attractive vdW force resulting in film rupture. However, if aqueous electrolyte is the film-forming bulk phase between the rising air bubble and the upper oil phase, the film always ruptured, even when a repulsive vdW interaction was predicted. We interpret these results as supporting the hypothesis that a short-ranged hydrophobic attraction determines the stability of the thin water film formed between an air phase and a nonpolar oil phase.

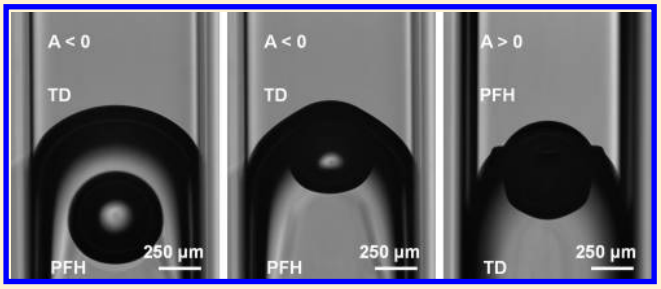

1. INTRODUCTION

The classical Derjaguin−Landau−Verwey−Overbeek (DLVO)[1] model accounts for the stability of colloidal systems in terms of the competition between electric double layer repulsion and van der Waals attraction between identical particles. The van der Waals (vdW) interaction[1,2] originates from quantum fluctuations of electric dipoles within the materials and operates between all physical bodies. Between identical bodies, this is an attraction that is responsible for the coagulation of solid suspensions, coalescence of emulsion droplets, and rupture of thin foam films. However, under certain combinations of dissimilar materials interacting through a third medium, the vdW interaction can be repulsive.

Earlier reports of the role of the vdW force on the stability of thin films include study of homologous alkane films on water[3] and liquid helium films on solid surface.[4] Direct force measurement using the atomic force microscopy (AFM) has been used to measure the repulsive vdW interaction between a solid colloidal probe attached to the AFM cantilever and a solid flat surface mediated by selected nonpolar organic solvents.[5−10] More recently, Tabor et al.[11] quantified the repulsive vdW interaction across water by dynamic force measurements using an air bubble as the AFM colloidal probe[12] and a flat solid surface of gold, mica or silica.

In this paper we aim to elucidate the role of repulsive vdW interaction in determining the stability of thin deformable liquid films trapped between the surface of a rising air bubble and an upper liquid−liquid interface. We use different combinations of immiscible liquids: water (refractive index, n = 1.33), a hydrocarbon oil that has a higher refractive index than water (tetradecane, $C_{14}H_{30}$, n = 1.43) and a fluorocarbon oil that has a lower refractive index than water (perfluorohexane, C_6F_{14}, n = 1.23). To suppress electric double layer electrostatic interactions, we use a concentrated aqueous electrolyte and adjust the pH to be near the isoelectric point of the air−water interface. Under such conditions it is expected that, under the DLVO paradigm, the form of the vdW interaction−repulsion or attraction will determine whether the rising bubble will stop at the fluid−fluid interface and be separated from it by a stable thin film or will break through the fluid−fluid interface.

2. EXPERIMENTAL SECTION

A small air bubble (diameter 50−700 μm) is released inside a liquid medium and rises under buoyancy toward a liquid−liquid meniscus that is concave down. A schematic diagram of the experimental setup is given in Figure 1. A glass container (cross section 4 cm × 4 cm, height 8 cm) is filled with a liquid that we refer to as the bulk liquid phase. A glass capillary with square cross-section (inner dimensions 1 mm × 1 mm) is mounted vertically at the top of the glass container with the lower open end immersed in the bulk liquid. The upper end of the

Received: March 9, 2014
Revised: April 21, 2014
Published: April 24, 2014

   dx.doi.org/10.1021/la500868y | Langmuir 2014, 30, 5162−5169

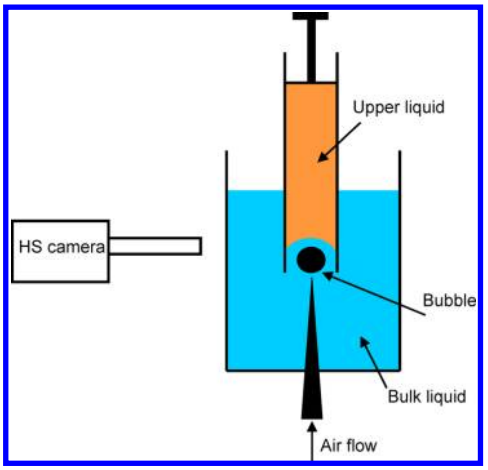

Figure 1. Schematic diagram of the experimental setup of a bubble (50−700 μm diameter) rising under buoyancy against a concave down fluid−fluid meniscus interface located inside a square capillary. The collision is recorded by high-speed video camera at 2000 fps.

capillary is connected to a 100 mL Hamilton syringe. The syringe is filled with the second liquid referred here as upper liquid phase. Using the syringe, the upper liquid is pushed down the capillary to form a concave down liquid−liquid meniscus interface close to the lower open end of the capillary. A bubble is released from the fine-end of a rounded glass capillary positioned at 1−2 mm below this liquid−liquid interface. Hereafter, each combination of liquids is specified in the following form: Air-Bulk Liquid-Upper Liquid.

The fine-end of the bubble release capillary with inner diameter 2−5 μm is manufactured using a glass-puller (Shutter instruments) that heats and pulls an original glass capillary of 50 μm inner diameter. The other end of the capillary is connected to an air compressor and a pressure regulator (AD 3000D from Iwashita Instruments Pte. Ltd.) by a plastic tube. Using combinations of different capillary fine-end diameters and pressure pulse durations we can release bubbles with diameters in the range of 50 to 700 μm.

To trap the rising bubble at the liquid−liquid interface with stability and reproducibility, a meniscus that is concave toward the rising bubble is preferred. Depending on the liquid combination such a meniscus can be arranged by making the inner walls of square glass capillary hydrophilic or hydrophobic. In the case where the upper liquid was water, the glass capillary was cleaned before use in a plasma-cleaner device (Harrick PDC-002) that will make it nearly fully water wet with a contact angle <10°, measured through the water. In the case where the bulk phase was water, the inside wall of the capillary was pretreated with a commercial hydrophobizing agent (Glaco Mirror Coat "Zero", Soft 99 Co.) that will make the glass surface superhydrophobic with water contact angle >160°, measured through the water.[13] For the air−perfluorohexane−tetradecane system, we used a hydrophilic capillary, and for the air−tetradecane−perfluorohexane system, we used a hydrophobic capillary to create the desired concave meniscus. We also used bromobenzene in a small number of experiments for the upper liquid. As the bromobenzene was found to affect the Glaco coating in the case of the air−water-bromobenzene system, we used glass capillaries hydrophobized with a silane reagent ((Trichloro (1H, 1H, 2H, 2H perfluorooctyl) silane, 97% Aldrich)) that gave a water contact angle of about 100°.

The oils used in the study were: tetradecane (TD; 99.5+%, olefin-free, Aldrich), perfluorohexane (PFH) in the commercial form known as PP1 (Flutec PP1; F2 Chemicals Ltd., U.K.), and bromobenzene (99+%, Aldrich). The oils were purified by passing them through a glass column filled with an activated magnesium silicate adsorbent (Florisil, Aldrich) before use. The aqueous electrolyte was made up using Millipore purified water and sodium perchlorate, $NaClO_4$ (99+%, Aldrich). The pH of the solution was adjusted by adding appropriate amounts of hydrochloric acid (HCl). The physical properties of the liquids used in the study are summarized in Table 1.

Table 1. Density (ρ), Shear Viscosity (μ), Surface Tension (γ), Refractive Index (n), and Dielectric Permittivity (ε) of the Liquid Phases Used[a]

liquid	ρ (kg/m^3)	μ (mPs)	γ (mN/m)	n	ε
water (0.5 M $NaClO_4$)	1000	0.95	72.4	1.33	76
tetradecane (TD)	760	2.21	26.5	1.43	2.1
perfluorohexane (PFH)	1700	1.10	11.9	1.25	1.7
bromobenze (BB)	1490	1.24	36.7	1.59	5.2
interfacial tension			γ_{12} (mN/m)		
water−TD			49.0		
water−PFH			56.0		
TD−PFH			6.3		

[a]The lower part of the table shows the interfacial tensions (γ_{12}) of the liquid combinations used.

The impact of the bubble on the liquid−liquid interface is recorded with a high-speed video camera (PhantomV1610 CMOS) connected to a long-distance microscope with a 10× objective (Mitutoyo) that gives a pixel resolution of 2.4 μm. The events of bubble impact, film drainage and the bubble crossing the fluid−fluid were recorded at a frame rate of 2000 fps. The use of a capillary with square cross-section eliminated optical distortions.

3. EXPECTED OUTCOME

Before we present experimental results let us consider the possible outcomes of the impact of the rising bubble against a liquid−liquid meniscus interface. As the bubble approaches the interface, hydrodynamic interaction will cause the bubble to decelerate as a film of the trapped bulk liquid of characteristic thickness, h, drains between the bubble and the meniscus. The rate of drainage of the film of bulk liquid will depend initially on the size of the bubble that determines the buoyancy force that drives the bubble. This buoyancy force is balanced against the hydrodynamic drag or resistance that depends on the viscosity of the bulk liquid and the upper liquid as well as the hydrodynamic boundary conditions on the bubble and meniscus surface. When the film is sufficiently thin, the sign and magnitude of the disjoining pressure due to colloidal surface forces will enter to determine the stability of the draining film. The extent of the deformation of the meniscus and bubble surface that is controlled by the respective interfacial tensions will together with the hydrodynamic and colloidal forces determine the local geometry of the draining thin film in a self-consistent manner.[14,15] However, the final equilibrium state will be determined by dependence of the disjoining pressure, $\Pi(h)$ on the film thickness, h.

If the disjoining pressure is attractive, $\Pi(h) < 0$ or not sufficiently repulsive, the draining film will eventually rupture and a three-phase (Air-Bulk liquid-Upper liquid) contact line will be formed and small bubbles will be trapped at the interface by capillary forces. However, if the bubble is sufficiently large for the buoyancy force to overcome the capillary force, the bubble will pass through the meniscus into the upper liquid.[16]

If the disjoining pressure, $\Pi(h)$ is repulsive (>0) and $\Pi(h) \rightarrow \infty$ as $h \rightarrow 0$, then if the bubble is not too large, that is the buoyancy force is not too large, a film of the bulk fluid of equilibrium thickness, h_{eq}, will be formed around the top of bubble between the air interface and the meniscus interface, and the bubble will be trapped there. However, if the bubble is sufficiently large for the buoyancy force to deform and break the meniscus, the bubble will pass through the meniscus into the upper liquid, carrying with it a film of the bulk fluid of

dx.doi.org/10.1021/la500868y | Langmuir 2014, 30, 5162−5169

thickness h_{eq} around its surface (see Appendix III, Supporting Information, for more details).

For the fluid systems used here, standard DLVO theory would predict that the disjoining pressure would be a sum of electric double layer (EDL) and van der Waals (vdW) interactions. In our experiments, there are no free charge carriers in the nonpolar phases. Our aqueous phase has a high added electrolyte concentration of 0.5 M $NaClO_4$ (Debye length = 0.3 nm) to screen out electrostatic interactions and we work at pH = 3.0, close to the isoelectric points of the bubble−water and water−oil interfaces to minimize the magnitude of the surface potential to below ∼5 mV.[17,18] Therefore, under such conditions, we expect the disjoining pressure to be dominated by the vdW interaction.

The vdW disjoining pressure can be written in the general form:

$$\Pi(h) = -\frac{A}{6\pi h^3} \tag{1}$$

where the Hamaker function A can be calculated using Lifshitz theory[2] in terms of an integration involving differences in the dielectric permittivity of the materials over imaginary frequencies. When the range of film thickness, h, is below the characteristic absorption wavelength of the materials, then A is the nonretarded Hamaker constant of the Air-Bulk Liquid-Upper Liquid system with $A < 0$ corresponding to vdW repulsion and $A > 0$ to attraction. For our systems that are composed of nonpolar and aqueous electrolyte at high electrolyte concentration, the zero-frequency contribution due to the high dielectric permittivity of water is screened out by the electrolyte and the characteristic absorption frequencies (or wavelengths) in the UV have comparable magnitudes.[1,19] Consequently, for our Air-Bulk Liquid-Upper Liquid systems, the sign of the Hamaker constant, A, that determines whether the vdW interaction is attractive or repulsive can be predicted from the relative magnitudes of the refractive indexes of the bulk, n_{bulk}, and upper, n_{upper} liquids:

$$\text{sign}\{A\} \sim \text{sign}\{(1 - n_{bulk})(n_{upper} - n_{bulk})\} \tag{2}$$

Essentially, if the refractive index of the bulk film-forming liquid is intermediate between that of air and the upper liquid, this asymmetric system will have a negative Hamaker constant and the vdW disjoining pressure would be repulsive. In such cases, the impact of the rising bubble against the interface between the bulk and the upper liquid is expected to result in the bubble being eventually trapped under the liquid meniscus with a stable film of the bulk liquid separating the bubble and the upper liquid.

On the other hand, if the refractive index of the bulk liquid is higher than that of the upper liquid, the Hamaker constant will be positive and the vdW interaction will be attractive. In such cases, the thin film of bulk liquid is expected to rupture and the bubble will either form a lens at the meniscus or pass through the meniscus and rise into the upper liquid.

In Table 2, we summarize values of the Hamaker constants determined from the refractive index and dielectric permittivity data given in Table 1, using the well-known approximate formula for the nonretarded Hamaker constant given by Israelachvili.[20] It is the sign of the Hamaker constants rather than their precise magnitudes that is the key feature in the present study. We distinguish between systems (see Table 2) in which (i) both the bulk and the upper liquids are nonpolar, (ii) the bulk film-forming liquid is nonpolar and the upper liquid is the aqueous electrolyte, and (iii) the bulk film-forming liquid is the aqueous electrolyte and the upper liquid is nonpolar.

Table 2. Nonretarded Hamaker Constant, A, of Different Systems of Air-Bulk Liquid-Upper Liquid Calculated[20] Using the Refractive Index, n, and Dielectric Permittivity, ε, Values in Table 1 and the Expected Stability of the Bulk Liquid Film between the Bubble and the Meniscus[a]

	systems	A (10^{-20} J)	expected film stability
i	Air-PFH-TD	−1.33	stable
	Air-TD-PFH	2.18	unstable
ii	Air-PFH-Water	−0.67	stable
	Air-TD-Water	1.08	unstable
iii	Air-Water-PFH	1.05	unstable
	Air-Water-TD	−0.65	stable
	Air-Water-BB	−2.09	stable

[a]The liquids are water (0.5 M $NaClO_4$, pH 3), tetradecane (TD), perfluorohexane (PFH), and bromobenzene (BB).

4. RESULTS AND DISCUSSION

4.1. Bubble Rise Terminal Velocities. Before we discuss experimental results of bubble collision with a liquid−liquid meniscus for the three different combinations of Air-Bulk Liquid-Upper Liquid we present results of measured terminal velocities of a rising bubble under buoyancy in the different liquids. Such results provide an indication of the hydrodynamic boundary condition and the mobility of the air−liquid interface. We measured the terminal rise velocities, U of bubbles of different radius, R in aqueous electrolyte (0.5 M $NaClO_4$, pH 3.0), tetradecane (TD), and perfluorohexane (PFH). As both the Reynolds number, $Re = 2\rho RU/\mu$, and the Weber number, $We = 2\rho RU^2/\gamma$, are small, the bubbles remain spherical as they rise. The bubble terminal velocity results are given in Figure 2 in terms of the Reynolds number.

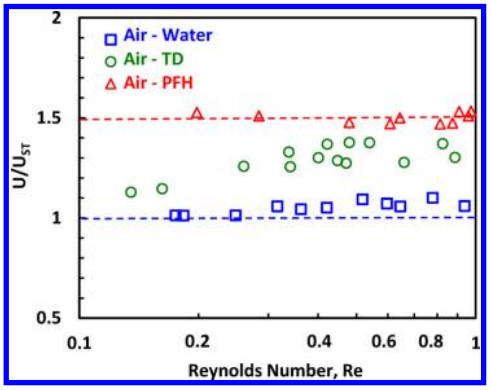

Figure 2. Variations of the terminal rise velocity scaled by the Stokes law terminal rise velocity, see eq 3, with the Reynolds number, $Re = 2\rho RU/\mu$, for air bubbles in water (squares, blue), tetradecane (TD; circles, green), and perfluorohexane (PFH; triangles, red). Lower dashed line (blue) corresponds to an immobile bubble surface and upper dashed line (red) to a fully mobile, zero tangential stress bubble surface.

If the air−liquid interface of the rising bubble is immobile and behaves like the surface of a solid sphere, the terminal velocity for small Re is given by the Stokes result, U_{ST}

$$U_{ST} = \frac{2\rho g R^2}{9\mu} \tag{3}$$

dx.doi.org/10.1021/la500868y | Langmuir 2014, 30, 5162−5169

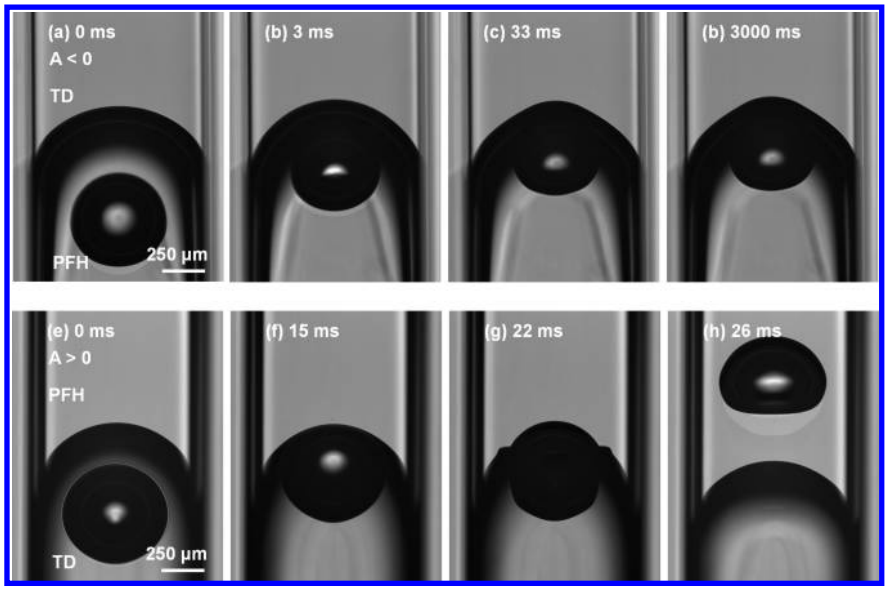

Figure 3. High-speed camera snapshots at selected times of a rising bubble impacting on the liquid−liquid meniscus in a square capillary for case (i) in Table 3 corresponding to the system of (a−d) Air-PFH-TD: (a) bubble rising toward the meniscus, (b) reached the interface, (c) coming to rest at the meniscus, and (d) the final stable equilibrium state; and (e−h) Air-TD-PFH system: (e) bubble rising toward and (f) reaching the interface followed shortly by (g) film rupture and finally (h) bubble passes into the upper phase; see Video 1.

On the other hand, if the air−liquid interface is fully mobile and has zero shear stress, the terminal velocity for the rising bubble at small *Re* is given by the Hadamard−Rubczynsky result, U_{HR} that is larger than the Stokes results by a factor (3/2):[21−23]

$$U_{HR} = \frac{\rho g R^2}{3\mu} \tag{4}$$

It is evident from Figure 2 that, for the bubble rise in water (0.5 M $NaClO_4$, pH 3.0), the data conforms to the Stokes law and suggests an immobile bubble surface. This result is consistent with the presence of trace amounts of surface active impurities that are known to immobilize the water surface except when a very rigorous cleaning procedure is applied.[22−24] For bubbles in perfluorohexane, the data show a fully mobile surface, which is also expected considering that the fluorocarbons are resistant to both polar and nonpolar contaminants. For tetradecane, the data indicate a partially mobile surface with a trend that larger bubbles appear to be more mobile. These experiments are indicative of the possible surfaces mobility conditions during the film draining; however, it should be noted that the mobility of the surface on a bubble rising at terminal velocity may be different to that during the film drainage process.[25]

4.2. Bubble Rise and Collision with Meniscus. We now turn to results for the outcome of bubble rise and collision with the meniscus in different systems of bulk and upper liquid systems, where in each case the vdW interaction may be either attractive (positive Hamaker constant) or repulsive (negative Hamaker constant), see Table 2. Examples of the impact events of the bubble at the meniscus for these three cases are given in the Supporting Information, Videos 1−3. For cases in which the thin bulk liquid film ruptures, we also estimate the coalescence or film drainage time, τ, defined as the time interval between when the bubble first arrives at the meniscus until film rupture is observed. If the drainage time, τ, is longer than a few ms, the precise time of first arrival at the meniscus is not important. Depending on the liquid system, τ can be a strong function of bubble size. We now present results of bubble rise and collision with the meniscus for different combinations of bulk liquid and upper liquid in the square capillary.

4.2.1. Air-Nonpolar Bulk-Nonpolar Upper Liquid Systems. When both the bulk film-forming liquid and the upper liquid are nonpolar liquids, case (i) in Table 2, the stability of the oil film between the bubble and the upper liquid is in accord with predictions based on the sign of the Hamaker constant for the vdW disjoining pressure. Specifically, the film is stable when the refractive index of the bulk film-forming phase is intermediate between that of air and the upper phase thus giving a negative Hamaker constant for vdW repulsion between the bubble and the meniscus. The left-hand frame of Video 1 shows a bubble impact experiment for the Air-PFH-TD system for which the repulsive vdW interaction due to a negative Hamaker constant ($A = -1.33 \times 10^{-20}$ J, see Table 2) is expected to sustain a stable thin film of perfluorohexane (PFH) between the air bubble and the tetradecane (TD) upper liquid. In contrast, the right-hand frame of Video 1 shows a bubble impact experiment in an Air-TD-PFH system where the bulk film-forming phase, TD, has the highest refractive index giving rise to a positive Hamaker constant ($A = 2.18 \times 10^{-20}$ J, see Table 2) and an attractive vdW interaction that resulted in film rupture.

In Figure 3a−d, we show snapshots from Video 1 for the Air-PFH-TD system and in Figure 3e−h for the Air-TD-PFH system. We see that, at the equilibrium state (Figure 3d), the bubble rests against the PFH-TD meniscus and is separated from it by a stable thin film. This stable configuration can be maintained for at least 24 h.

4.2.2. Air-Nonpolar Bulk-Water Systems. For the systems in case (ii) of Table 2, the Upper Liquid in the capillary is the aqueous electrolyte (0.5 M $NaClO_4$, pH = 3.0) and the bulk liquid is nonpolar oil. When the bulk liquid is perfluorohexane (PFH), we have a negative Hamaker constant and a repulsive vdW disjoining pressure that is expected to stabilize the PFH film. On the other hand, when the bulk liquid is tetradecane (TD), the Hamaker constant is positive, and that gives an attractive vdW disjoining pressure that is expected to rupture

dx.doi.org/10.1021/la500868y | *Langmuir* 2014, 30, 5162−5169

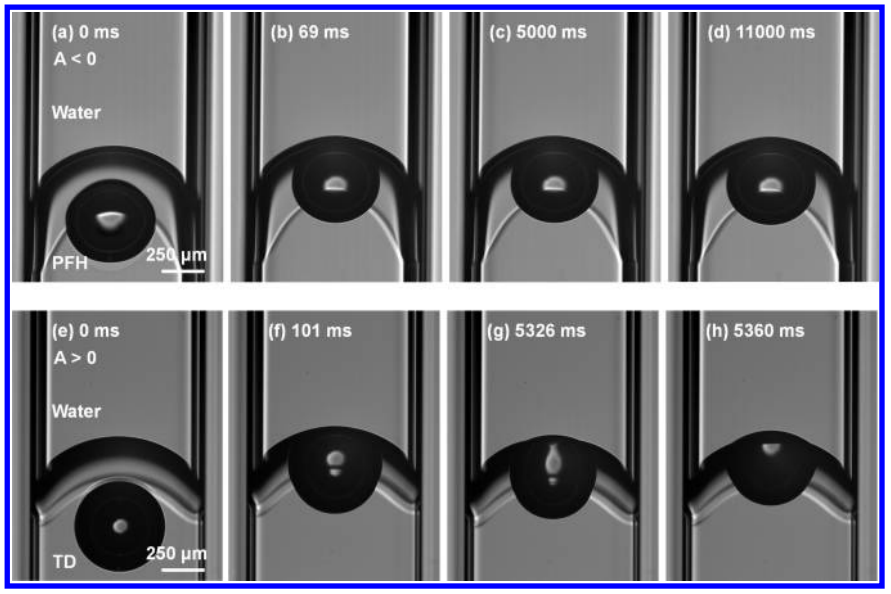

Figure 4. High-speed camera snapshots at selected times of a rising bubble impact for (a–d) the Air-PFH-Water system: (a) bubble rising toward the meniscus, (b) reached the interface, (c) coming to rest at the meniscus, and (d) the final equilibrium state with a thin equilibrium film between the bubble and the meniscus; and (e–h) Air-TD-Water system: (e) bubble rising toward and (f) reaching the interface, followed by (g) a long film drainage process before film rupture with (h) the bubble trapped as a lens at the equilibrium at the meniscus; see Video 2.

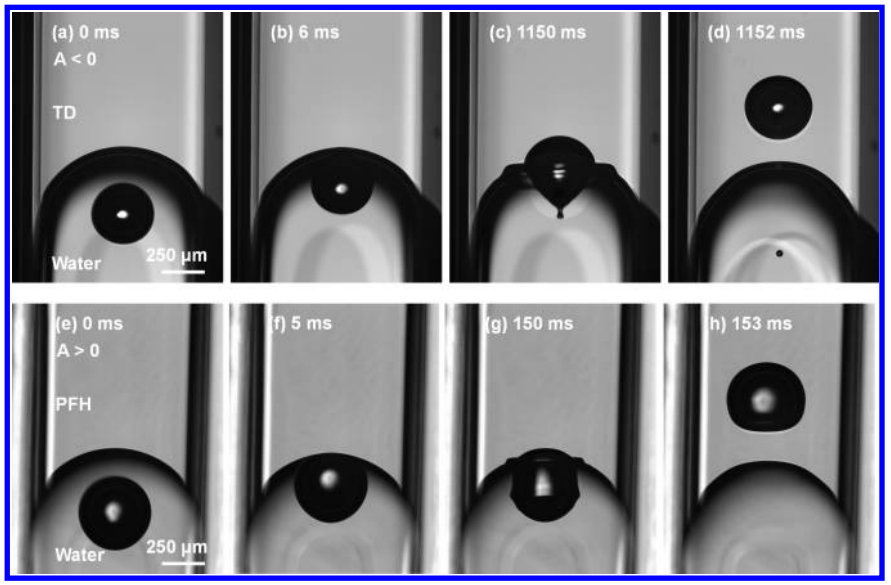

Figure 5. High-speed camera snapshots at selected times from Video 3 of a rising bubble impact for (a–d) the Air-Water-TD system: (a) bubble rising toward the meniscus, (b) reached the interface (c, d) rupture of the water film after a long drainage time and the bubble passes into the upper TD phase; and (e–h) Air-Water-PFH system: (e) bubble rising toward and (f) reached the interface followed by (g) a shorter film drainage process before film ruptures with (h) the bubble passing into the upper PFH phase.

the TD film between the bubble and the meniscus (see Table 2).

In Video 2, we see that the theoretical predictions of film stability base on a consideration of the vdW interaction are fully realized. For the Air-PFH-Water system, see also snapshots in Figure 4a–d, the repulsive vdW disjoining pressure indicated by a negative Hamaker constant ($A = -0.67 \times 10^{-20}$ J, see Table 2) is able to maintain a stable PFH film that separates the bubble and the meniscus in the equilibrium state (Figure 4d). On the other hand, for the Air-TD-Water system (see also snapshots in Figure 4e–h) that has a positive Hamaker constant ($A = 1.08 \times 10^{-20}$ J, see Table 2), the TD film takes between 0.1 to 10 s to drain, depending on the bubble size. Following film rupture, the bubble became trapped as an air lens (Figure 4h) at the TD–water meniscus as a result of the relative magnitudes of the interfacial tensions.[26]

So far, the stability or rupture behavior of the liquid systems in cases (i) and (ii) (Table 2) follow the predictions based on the sign of the Hamaker constant.

4.2.3. Air-Water Bulk-Nonpolar Upper Liquid Systems. We now consider systems in which aqueous electrolyte (0.5 M $NaClO_4$, pH = 3.0) is the bulk film-forming liquid-case (iii) of Table 2. When the upper liquid is perfluorohexane (PFH)-Air-Water-PFH, the Hamaker constant is positive and the vdW disjoining pressure is attractive. The aqueous film is observed to rupture, as expected, after a drainage time of 50 to 200 ms.

dx.doi.org/10.1021/la500868y | *Langmuir* 2014, 30, 5162–5169

When the upper liquid is tetradecane (TD), the vdW disjoining pressure of the Air-Water-TD system is repulsive due to the negative Hamaker constant. But in spite of this, the water film still ruptured, albeit after a longer drainage time of 0.5 to 2 s; see Video 3 and snapshots in Figure 5. Thus, contrary to all previous cases, the repulsive vdW disjoining pressure of the Air-Water-TD system is unable to maintain film stability. To increase the magnitude of the vdW repulsion, we used bromobenzene (BB) as the upper liquid for which the Air-Water-BB system is expected to give a negative Hamaker constant of larger magnitude than the Air-Water-TD system (see Table 2). Nevertheless, the aqueous film remains unstable with drainage times comparable to the Air-Water-PFH and Air-Water-TD systems.

In Table 3, we summarize the observed range of coalescence times for different combination of Air-Bulk Liquid-Upper Liquid systems. For cases (i) and (ii) in which the bulk film-forming phase is nonpolar, the stability of the film can be inferred from the sign of the Hamaker constant that determines whether the vdW disjoining pressure is repulsive or attractive. However, when aqueous electrolyte is the bulk film-forming liquid, film rupture is always observed, contrary to predictions based on considering only vdW interactions.

Table 3. Observed Coalescence Times, τ, for Different Cases of Air-Bulk Liquid-Upper Liquid Systems and the Final State of the Bubble

	systems	A (10^{-20} J)	τ (ms)	final state
i	Air-PFH-TD	−1.33	stable	film
	Air-TD-PFH	2.18	5−15	crosses meniscus
ii	Air-PFH-Water	−0.67	stable	film
	Air-TD-Water	1.08	100−9000	lens
iii	Air-Water-PFH	1.05	50−300	crosses meniscus
	Air-Water-TD	−0.65	500−2000	crosses meniscus
	Air-Water-BB	−2.09	20−200	crosses meniscus

4.3. Drainage Times Dependences. Detail modeling of the dynamics of film drainage and coalescence times of thin liquid films required experimental measurements of (i) the time evolution of the film shape and thickness using, for example, interferometry methods or (ii) the time evolution of the force between the bubble and the interface as in AFM force measurement experiment.[14,15] The only parameter we can estimate in our experiments at present is the approximate time between the bubble initial contact with the interface and the film rupture to which we refer as drainage time, τ. This is insufficient for accurate modeling of the film evolution. Therefore, we limit ourselves to a more general analysis of the observed drainage times trends using simplified film thinning theories.

A further limitation to the quantitative interpretation of the drainage times in our experiment is precise knowledge of the hydrodynamic boundary condition at the liquid−liquid and gas−liquid interfaces. At the air−water or oil−water interface, the immobile or no-slip boundary condition holds due to trace surface active contaminations that are almost always present in the water phase.[22−24] However, for air−oil or for oil−oil interface, a partial or full slip boundary condition could apply as indicated in our bubble terminal rise velocity experiments discussed in the previous section (see Figure 2). Thus, we consider two limiting cases: (I) flat disk model with nonslip boundary conditions,[27−29] detailed in Appendix I, which gives the upper limit estimation for the drainage times, and (II) full slip boundary condition on nondeformable surface,[30,31] detailed in Appendix II, which gives the low limit estimation for the drainage times. We are cognizant that these are highly simplified models that can at best provide an order of magnitude estimate of the drainage times or perhaps just the general trend in the variation of drainage time with bubble size.

In Figure 6, we show the observed dependence of drainage time on the bubble radius where tetradecane is the bulk film-forming phase and the vdW disjoining pressure is attractive. As discussed in the previous section in that case, the general prediction of the film stability is in accordance with the predicted sign of the vdW interaction. There are two trends that are observed: (i) the range of the drainage times for the Air-TD-PFH system is much shorter compared to the range for the Air-TD-Water system: 5−10 ms vs 100−9000 ms, and (ii) the Air-TD-PFH system shows only a week dependence on the bubble radius, whereas the Air-TD-Water shows an exponential dependence on the bubble radius.

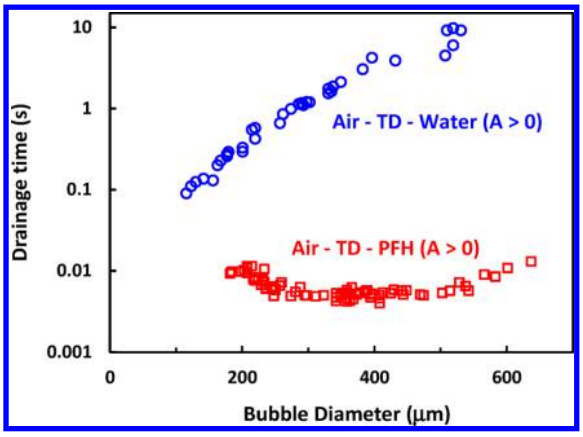

Figure 6. Thin liquid film drainage time dependence on the nondeformed bubble diameter for the case of Air-TD-PHF system (squares, red) and Air-TD-Water system (circles, blue), both cases with attractive vdW disjoining pressure.

Taking typical values for the interfacial tension and Hamaker constant for the Air-TD-Water system (Tables 1 and 2) using the flat disc, no-slip boundary conditions model (Appendix I), we can obtain the experimentally observed range of drainage times of 0.1 to 10 s. This model however predicts a linear dependence on the bubble radius and not the stronger exponential dependence of the experimental data. On the other hand, the shorter drainage time range of about 5 to 10 ms for the Air-TD-PFH system can be obtained using the full-slip, nondeformable surface model (Appendix II) that also predicts that the drainage time to be independent of the bubble radius. As discussed above, limitations of our experiment such as the unknown time-evolution of film thickness and the precise nature of the surface boundary conditions do not allow a more conclusive interpretation of the drainage time dependences shown in Figure 6.

In Figure 7 we show the observed dependence of the drainage time on the bubble radius in the case of where water is the bulk film-forming phase. In both cases the films are unstable which contradicts prediction of film stability based on the sign of the vdW force for the Air-Water-TD system. Usually the instability of thin aqueous liquid films trapped between two hydrophobic phases is explained by invoking the role of

dx.doi.org/10.1021/la500868y | Langmuir 2014, 30, 5162−5169

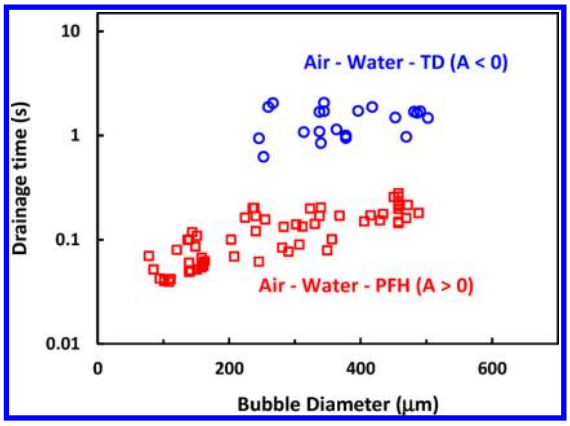

Figure 7. Thin liquid film drainage time dependence on the nondeformed bubble diameter for the case of Air-Water-PHF (attractive vdW) system (squares, red) and Air-Water-TD (repulsive vdW) system (circles, blue).

attractive hydrophobic forces. In spite of numerous experimental and theoretical studies the precise range and intensity of the hydrophobic attraction remains a topic of current interest.[32−38] Recently, Tabor et al.[38] measured the hydrophobic force between two oil droplets in water under well-controlled conditions. By selectively suppressing electrical double layer interactions though the use of high salt and adjusting sign and magnitude of the van der Waals interaction by tuning the refractive indices of the oil droplets, the hydrophobic attraction can be quantified by studying how the drops coalesce under different hydrodynamic conditions. Our experiments are indicative for the operation of this attraction for the air−water−oil system and that it is strong enough to dominate a repulsive vdW interaction with Hamaker constant in the range $\sim 10^{-20}$ J.

5. CONCLUSIONS

Here we have examined the stability of thin liquid films that are expected to be determined by attractive or repulsive vdW interaction by observing the impact of rising bubble on a liquid−liquid interface. We found that when the film-forming phase is nonpolar oil, the film stability can always be predicted from the sign of the vdW interaction with a repulsive vdW force resulting in a stable film. In the case of aqueous films formed between the bubble and the nonpolar oil phase, the repulsive vdW interaction alone could not stabilize the film and such an aqueous film always ruptures. This is interpreted as an indication that the attractive hydrophobic force between the bubble and the nonpolar oil phase rather than the repulsive vdW interaction is dominating the thin aqueous films stability in these systems. In addition, we have obtained some intriguing dependence of the film drainage time of unstable films on bubble size. Although the present results cannot be interpreted quantitatively, the experimental approach can be refined to include direct measurements of the spatial geometry and time variations of the thin aqueous film, as well as interfacial mobility and hydrodynamic boundary condition. Such detailed information will permit accurate quantitative comparisons with a dynamic film drainage model that takes into account the hydrodynamics of film drainage and film deformation under capillary and surface forces.[14,15]

■ ASSOCIATED CONTENT

Supporting Information

Appendix I: Stefan-Reynolds Flat Disk Model, Stokes flow with at least one interface is no-slip. Appendix II: Potential flow with BOTH interfaces obey the slip boundary condition. Appendix III: Disjoining pressure between two deformable interfaces. Video 1: Bubble impact experiment in an Air-PFH-TD (left-side) and Air-TD-PFH (right-side) system. The real time duration of the video clip is 125 ms. Video 2: Bubble impact experiment in an Air-PFH-Water (left-side) and Air-TD-Water (right-side) system. The real time duration of the video clip is 7500 ms. Video 3: Bubble impact experiment in an Air-Water-TD (left-side) and Air-Water-PFH (right-side) system. The real time duration of the video clip is 1222 ms. This material is available free of charge via the Internet at http://pubs.acs.org.

■ AUTHOR INFORMATION

Corresponding Author

*Tel.: +96628082119. E-mail: ivanuriev.vakarelski@kaust.edu.sa.

Notes

The authors declare no competing financial interest.

■ ACKNOWLEDGMENTS

E.Q.L. is grateful for a SABIC Postdoctoral Fellowship. This work is supported in part by an Australian Research Council Discovery Project Grant to D.Y.C.C.

■ REFERENCES

(1) Israelachvili, J. N. *Intermolecular and Surface Forces*, 3rd ed.; Academic Press Ltd.: San Diego, 2011.
(2) Dzyaloshinskii, I. E.; Lifshitz, E. M.; Pitaevskii, L. P. The general theory of van der Waals forces. *Adv. Phys.* **1961**, *10*, 165−209.
(3) Hauxwell, F.; Ottewill, R. H. A study of the surface of water by hydrocarbon adsorption. *J. Colloid Interface Sci.* **1970**, *34*, 473−479.
(4) Sabisky, E. S.; Anderson, C. H. Verification of the Lifshitz theory of the van der Waals potential using liquid-helium films. *Phys. Rev. A* **1973**, *7*, 790−806.
(5) Hutter, J. L.; Bechhoefer, J. Manipulation of van der Waals force to improve imaging resolution in atomic-force microscopy. *J. Appl. Phys.* **1993**, *73*, 4123−4129.
(6) Milling, A.; Mulvaney, P.; Larson, I. Direct measurement of repulsive van der Waals interactions using an atomic force microscope. *J. Colloid Interface Sci.* **1996**, *180*, 460−465.
(7) Meurk, A.; Luckham, P.; Bergström, L. Direct measurement of repulsive and attractive van der Waals forces between inorganic materials. *Langmuir* **1997**, *13*, 3896−3899.
(8) Lee, S.-W.; Sigmund, W. M. AFM study of repulsive van der Waals forces between Teflon AF thin film and silica or alumina. *Colloids Surf., A* **2002**, *204*, 43−50.
(9) Feiler, A. A.; Bergström, L.; Rutland, M. W. Superlubricity using repulsive van der Waals forces. *Langmuir* **2008**, *24*, 2274−2276.
(10) Munday, J. N.; Capasso, F.; Parsegian, V. A. Measured long-range repulsive Casimir−Lifshitz forces. *Nature* **2009**, *457*, 170−173.
(11) Tabor, R. F.; Manica, R.; Chan, D. Y. C.; Grieser, F.; Dagastine, R. R. Repulsive van der Waals forces in soft matter: Why bubbles do not stick to walls. *Phys. Rev. Lett.* **2011**, *106*, 064501.
(12) Vakarelski, I. U.; Manica, R.; Tang, X. S.; O'Shea, S. J.; Stevens, G. W.; Grieser, F.; Dagastine, R. R.; Chan, D. Y. C. Dynamic interactions between microbubbles in water. *Proc. Natl. Acad. Sci. U.S.A.* **2010**, *107*, 11177−11182.
(13) Vakarelski, I. U.; Patankar, N. A.; Marston, J. O.; Chan, D. Y. C.; Thoroddsen, S. T. Stabilization of Leidenfrost vapour layer by textured superhydrophobic surfaces. *Nature* **2012**, *489*, 274−277.

(14) Chan, D. Y. C.; Manica, R.; Klaseboer, E. Film drainage and coalescence between deformable drops and bubbles. *Soft Matter* **2011**, *7*, 2235−2264.
(15) Chan, D. Y. C.; Klaseboer, E.; Manica, R. Theory of nonequilibrium force measurements involving deformable drops and bubbles. *Adv. Colloid Interface Sci.* **2011**, *165*, 70−90.
(16) Li, E. Q.; Al-Otaibi, S. A.; Vakarelski, I. U.; Thoroddsen, S. T. Satellite formation during bubble transition through an interface between immiscible liquids. *J. Fluid Mech.* **2014**, *744*, R1.
(17) Marinova, K. G.; Alargova, R. G.; Denkov, N. D.; Velev, O. D.; Petsev, D. N.; Ivanov, I. B.; Borwankar, R. P. Charging of oil−water interfaces due to spontaneous adsorption of hydroxyl ions. *Langmuir* **1996**, *12*, 2045−2051.
(18) Clasohm, L. Y.; Vakarelski, I. U.; Dagastine, R. R.; Chan, D. Y. C.; Stevens, G. W.; Grieser, F. Anomalous pH dependent stability behavior of surfactant-free nonpolar oil drops in aqueous electrolyte solutions. *Langmuir* **2007**, *23*, 9335−9340.
(19) Bergström, L. Hamaker constants of inorganic materials. *Adv. Colloid Interface Sci.* **1997**, *70*, 125−169.
(20) Israelachvili, J. N. *Intermolecular and Surface Forces*, 3rd ed.; Academic Press Ltd.: San Diego, 2011; p 260.
(21) Levich, V. G. *Physicochemical Hydrodynamics*; Prentice−Hall International Series in the Physical and Engineering Sciences; Prentice−Hall: Englewood Cliffs, 1962; p 700.
(22) Kelsall, G. H.; Tang, S.; Smith, A. L.; Yurdakul, S. Measurement of rise and electrophoretic velocities of gas bubbles. *J. Chem. Soc., Faraday Trans.* **1996**, *92*, 3879−3885.
(23) Parkinson, L.; Sedev, R.; Fornasiero, D.; Ralston, J. The terminal rise velocity of 10−100 μm diameter bubbles in water. *J. Colloid Interface Sci.* **2008**, *322*, 168−172.
(24) Henry, C. L.; Parkinson, L.; Ralston, J.; Craig, V. S. J. A mobile gas−water interface in electrolyte solutions. *J. Phys. Chem. C* **2008**, *112*, 15094−15097.
(25) Manica, R.; Hendrix, M. H. W.; Klaseboer, E.; Ohl, C.-D.; Chan, D. Y. C. Effects of hydrodynamic film boundary conditions on bubble−wall impact. *Soft Matter* **2013**, *9*, 9755−9758.
(26) Neeson, M. J.; Tabor, R. F.; Grieser, F.; Dagastine, R. R.; Chan, D. Y. C. Compound sessile drops. *Soft Matter* **2012**, *8*, 11042−11050.
(27) Stefan, J. Studies in apparent adhesion (in German) *Sitzber Akad Wiss Wien. Abh. Dtsch. Akad. Wiss. Berlin, Math.-Naturwiss. Kl.* **1874**, *69*, 713−735.
(28) Reynolds, O. On the theory of lubrication and its application to Mr. Beauchamp Tower's experiments, including an experimental determination of the viscosity of olive oil. *Philos. Trans. R. Soc. London* **1886**, *177*, 157−234.
(29) Ivanov, I.; Dimitrov, D. *Thin Liquid Films*; Marcel Dekker: New York, 1988.
(30) Miloh, T. Hydrodynamics of deformable contiguous spherical shapes in an incompressible inviscid fluid. *J. Eng. Math.* **1977**, *11*, 349−372.
(31) Kharlamov, A. A.; Chára, Z.; Vlasák, P. Hydraulic formulae for the added masses of an impermeable sphere moving near a plane wall. *J. Eng. Math.* **2007**, *62*, 161−172.
(32) Ducker, W. A.; Xu, Z.; Israelachvili, J. N. Measurements of hydrophobic and DLVO forces in bubble-surface interactions in aqueous solutions. *Langmuir* **1994**, *10*, 3279−3289.
(33) Butt, H.-J. Technique for measuring the force between a colloidal particle in water and a bubble. *J. Colloid Interface Sci.* **1994**, *166*, 109−117.
(34) Fielden, M. L.; Hayes, R. A.; Ralston, J. Surface and capillary forces affecting air bubble-particle interactions in aqueous electrolyte. *Langmuir* **1996**, *12*, 3721−3727.
(35) Kralchevsky, P. A.; Danov, K. D.; Angarska, J. K. Reply to comment on "Hydrophobic forces in the foam films stabilized by Sodium Dodecyl Sulfate: Effect of electrolyte" and subsequent criticism. *Langmuir* **2008**, *24*, 2953−2953.
(36) Hammer, M. U.; Anderson, T. H.; Chaimovich, A.; Shell, M. S.; Israelachvili, J. N. The search for the hydrophobic force law. *Faraday Discuss.* **2010**, *146*, 299−308.
(37) Wang, L.; Sharp, D.; Masliyah, J.; Xu, Z. Measurement of interactions between solid particles, liquid droplets, and/or gas bubbles in a liquid using an integrated thin film drainage apparatus. *Langmuir* **2013**, *29*, 3594−3603.
(38) Tabor, R. F.; Wu, C.; Grieser, F.; Dagastine, R. R.; Chan, D. Y. C. Measurement of the hydrophobic force in a soft matter system. *J. Phys. Chem. Lett.* **2013**, *4*, 3872−3877.